Available online at www.sciencedirect.com
ScienceDirect
Journal of Nuclear Materials 372 (2008) 1–15
journal of nuclear materials
www.elsevier.com/locate/jnucmat

A comprehensive model to describe radiolytic processes in cement medium

P. Bouniol [a,*], E. Bjergbakke [b]

[a] Commissariat à l'Energie Atomique, DEN/DPC, CEA-Saclay, 91191 Gif sur Yvette cedex, France
[b] Risoe National Laboratory, DK-4000 Roskilde, Denmark

Received 7 May 2006; accepted 11 October 2006

Abstract

Basic mechanisms controlling the radiolysis in cementitious matrices are reviewed in the specific context of the gamma irradiation, in closed system without upper vapour space, at 25 °C, with a pore solution representative of a Portland cement paste. A general survey of data corresponding to each phenomenological area is given, particularly with a list of reactions for alkaline medium and a revised description of equilibria related to calcium hydroxide. Simulations as a function of dose rate, liquid saturation in the porosity or initial amount of H_2 are carried out with the *CHEMSIMUL* code. They show the existence of several ways in the radiolysis regulation involving calcium peroxide octahydrate precipitation, a law of mass action through the bulk general system, or the particular activation of an Allen's type chain reaction. This latter seems faster in alkaline medium (pH > 13) where radicals $H^{\cdot}$ and $OH^{\cdot}$ are, respectively, replaced by e^-_{aq} and $O^{\cdot -}$. Excepted when a strong reducing agent is initially present, O_2 is normally produced by radiolysis and $CaO_2 \cdot 8H_2O$ cannot be responsible of its disappearance.

PACS: 82.20.Wt; 82.33.Ln; 82.40.Qt; 82.50.Kx

1. Introduction

Widely employed in nuclear industry, concretes, mortars and grouts can be subjected to radiations in a number of situations (structural concretes and shield materials, matrices for conditioning or embedding of radioactive wastes). Residual pore water in these materials is affected by a decomposition (radiolysis) whose intensity is a function of many factors: dose rate, radiation type, and initial chemical composition of the pore solution. With the in situ emission of hydrogen gas or escape into the operational area, consequences of the radiolysis create problem of safety whose analysis is essentially based on the accurate evaluation of the H_2 source-term, in other words on the complete description of the radiolysis and its associated phenomena. This evaluation is made particularly difficult because of the composite and porous character of the cementitious materials where the presence of gas and solid phases strongly interfere with the pore water radiolysis. In a first approach [1], the interaction between $Ca(OH)_2$ (present in hydrated cement) and H_2O_2 (radiolytic product) to form the calcium peroxide octahydrate has been evoked in order to complete the already known reaction mechanisms and to try to explain the O_2 disappearance, frequently observed under γ irradiation, by an immobilization in the form of solid peroxide. The formation of $CaO_2 \cdot 8H_2O$ may be the mechanism of O_2 removal. However, this conclusion seems to be now erroneous insofar as:

- the solubility and the precipitation threshold were not taken into account (*a minima*, solubility product of the solid must be exceeded before $CaO_2 \cdot 8H_2O$ precipitation),
- the reality of mineralogical equilibrium has been neglected (the heterogeneous equilibrium solid-solution

* Corresponding author.

0022-3115/$ - see front matter © 2006 Published by Elsevier B.V.
doi:10.1016/j.jnucmat.2006.10.004

forbids the concentration of peroxide ions, in consequence the O_2's one too, to diminish as far as zero).

At the origin of a virtual oxygen pump, these oversights have been corrected in a more recent monograph [2] describing the different basic phenomena and their coupling. On the other hand, in order to simulate radiolysis at longer or shorter times, this work must reconcile reactions usually neglected for their slowness (Haber–Weiss reactions) but involving indirectly the production of H_2 *in fine*.

Coming back to the understanding of the basic mechanisms of radiolysis within the cementitious matrices, we will here restrict ourselves to a chemical point of view, starting from a standard configuration: matrix of ordinary Portland cement (OPC) subjected to a gamma irradiation in closed system, at a temperature of 25 °C. The necessity of working out a model integrating the largest number of mechanisms is an essential step in the interpretation of experiments which are carried out with this type of cement. The physico-chemical complexity of blended cements (for example blast furnace slag-based cements with presence of S^{2-}) does not yet allow such an approach.

2. Composition of the pore solution

The residual liquid occupying the porosity of the cementitious material is not pure water but an aqueous solution in equilibrium with the constituent minerals of the hydrated cement paste ($Ca(OH)_2$, hydrated hydroxi-silicate and sulfo-aluminate of calcium), added up with labile elements (Na, K). In first approximation, the composition of this liquid is assimilated with a solution of NaOH at pH > 13, equilibrated with $Ca(OH)_2$ (portlandite). Considering the case of a reference liquid with 0.24 mol/kg of sodium, molal concentrations of these species in solution (Table 1) can be calculated with the help of the data in Table 2. These data result themselves from a refinement of the constants related to the description of a solution equilibrated with portlandite. Calculations use electroneutrality equation, ionic product of water [3], pH and total calcium of the saturated solution [4,5], complexation constants of $CaOH^+$ and $NaOH^0$ [6]. Activity coefficients are calculated from Eq. (1) (Davies formula), with $a = 0.5092$ and 2.0368, respectively, for mono- and bi-charged ions, that is justified for a ionic strength $I < 0.3$ mol/kg

$$\gamma = 10^{-a\left(\frac{\sqrt{I}}{1+\sqrt{I}}-0.3I\right)}. \tag{1}$$

Water activity is defined in first approximation by its molar fraction

$$(H_2O) = \frac{[H_2O]}{[H_2O] + \sum_i [\text{solute}_i]}, \tag{2}$$

where $[H_2O] = \frac{1}{M_{H_2O}} = 55.5084\ \text{mol/kg}_{\text{solvent}}$.

Taking everything into account (iterative calculation), total concentration of the solutes, ionic strength and pH of the solution are, respectively, equal to

$$\sum_i [\text{solute}_i] = 4.6742 \times 10^{-1}\ \text{mol/kg}_{\text{solvent}}, \tag{3}$$

$$I = \frac{1}{2}\sum_i z_i^2 [\text{solute}_i] = 2.257 \times 10^{-1}\ \text{mol/kg}_{\text{solvent}}, \tag{4}$$

$$\text{pH} = 13.225. \tag{5}$$

In addition, the solution is characterized by a density and a mass of solutes per mass of solvent equal to

$$\rho_{\text{liq}} = 1007.71\ \text{kg/m}^3, \tag{6}$$

$$\sum_i M_i [\text{solute}_i] = 9.778 \times 10^{-3}\ \text{kg}_{\text{solute}}/\text{kg}_{\text{solvent}}. \tag{7}$$

Table 1
Calculated molal concentrations of species in a simplified pore solution of OPC at 25 °C (mol/kg$_{water}$)

Cations	Molecules	Anions
$[H_3O^+] = 8.021 \times 10^{-14}$	$[H_2O] = 55.5084$	$[OH^-] = 2.250 \times 10^{-1}$
$[Na^+] = 2.229 \times 10^{-1}$	$[NaOH^0] = 1.705 \times 10^{-2}$	
$[CaOH^+] = 6.837 \times 10^{-4}$	$[Ca(OH)_2^0] = 1.038 \times 10^{-3}$	
$[Ca^{2+}] = 6.902 \times 10^{-4}$		

Table 2
Mineralogical and complexation equilibria used in the calculation of the pore solution at 25 °C

Species	Equilibrium constant	Value	Ref.
Solvent H_2O	$K_w = [H_3O^+][OH^-] \cdot \gamma_1^2 \cdot \left(\frac{[H_2O]+\sum[\text{solute}_i]}{[H_2O]}\right)^2$	$10^{-13.9953}$	[3]
Portlandite $Ca(OH)_2$	$K_{\text{port}} = [Ca^{2+}][OH^-]^2 \cdot \gamma_2 \cdot \gamma_1^2$	$10^{-5.2338}$	This work
Complex $CaOH^+$	$K_1 = \frac{[CaOH^+]}{[Ca^{2+}][\ OH^-] \cdot \gamma_2}$	$10^{1.1618}$	[6]
Complex $Ca(OH)_2^0$	$K_2 = \frac{[Ca(\ OH)_2^0]}{[CaOH^+][OH^-] \cdot \gamma_1^2}$	$10^{1.0882}$	This work
Complex $NaOH^0$	$K_3 = \frac{[NaOH^0]}{[Na^+][\ OH^-] \cdot \gamma_1^2}$	$10^{-0.2096}$	[6]

These two data allow to translate molalities into molarities with the help of a coefficient for concentration units conversion (CUC)

$$\mathrm{CUC} = \frac{10^{-3}\rho_{\mathrm{liq}}}{1 + \sum_i M_i[\mathrm{solute}_i]} = 0.998\ \mathrm{kg}_{\mathrm{solvent}}/\mathrm{dm}^3_{\mathrm{solution}}. \quad (8)$$

The high pH of the solution forces a fairly low concentration of the calcium (2.412×10^{-3} mol/kg) where the neutral complex $Ca(OH)^0_2$ is the dominant aqueous species. It is recalled that the concentration of this species, independent of the pH, is determined by a product of constants (see Table 2)

$$[Ca(OH)^0_2] = K_{\mathrm{port}} \cdot K_1 \cdot K_2. \quad (9)$$

3. Primary products

3.1. Primary production

Within 10^{-7} to 10^{-6} s as the gamma radiation passed, the water decomposition leads to the formation of eight primary species (4 molecules: H_2, H_2O_2, OH^-, H_3O^+ and 4 radicals: e_{aq}^-, $H^\bullet$, $OH^\bullet$, $HO_2^\bullet$) uniformly distributed in the solution (homogeneous step). At this stage, the primary production of these species proceeds from a zero order kinetics, i.e. independent of the concentrations or the amount of solvent. Keeping H_2 for example, the primary production kinetics in solution is defined by

$$\left(\frac{\mathrm{d}[H_2]}{\mathrm{d}t}\right)_{\mathrm{prim}} = \frac{\mathrm{CUC}}{c_{\mathrm{en}}\mathscr{N}_A} \times D'_{H_2O} \times G_{H_2}\ \mathrm{mol\ dm^{-3}\ s^{-1}}, \quad (10)$$

where D'_{H_2O} is the dose rate in water (J kg^{-1}_{water} s^{-1} = Gy/s), G_{H_2} is the primary yield of H_2 (molecule/heV[1]), $c_{en} = 1.602176462 \times 10^{-17}$ J/heV is an energy conversion factor and $\mathscr{N}_A = 6.02214199 \times 10^{23}$ is the Avogadro number. Because of the dispersion of the interstitial solution within the porous material, the interaction radiation-material affects the entirety of the solid and liquid phases, and the dose rate in water is more correctly described by the kerma rate (Kinetic Energy Released in MAtter). This latter takes into account the sum of the initial kinetic energy of every charged ionizing particles induced by incident photons, including Compton electrons. Considering the kerma rate for the two constituent atoms of the solvent, the dose rate in water is given by

$$D'_{H_2O} = \frac{\mathscr{N}_A}{\mathscr{M}_{H_2O}}(2\mathrm{kerma}'_H + \mathrm{kerma}'_O)\mathrm{Gy/s}, \quad (11)$$

where $\mathscr{M}_{H_2O} = 1\,801\,528 \times 10^{-3}$ kg/mol is the water molar mass, kerma'_H and kerma'_O are the respective kerma rates on the atoms H and O (J $atom^{-1}$ s^{-1}).

[1] heV = 100 eV.

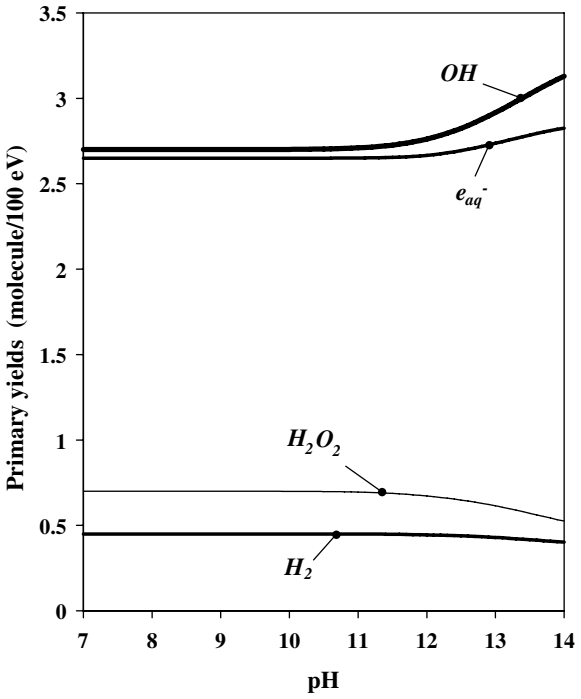

Fig. 1. Evolution of gamma primary yields for the main radiolytic species at 25 °C as a function of pH.

3.2. Primary yields

Particularly studied with gamma radiation, evolution of the primary yields is sensitive in alkaline medium, especially in the pH 12–14 interval where radicals products show a fairly pronounced increase when molecular products show a more moderated decrease (Fig. 1). In consideration of the variability of the alkali contents in industrial cements, this means that there is no standard value of the primary yields for cement matrices (so, G_{H_2} can vary from 0.435 to 0.384 between pH 12.45 and 14). Concerning the pH of the reference pore solution, plots fitted from experimental values of Hayon [7] and Haïssinsky [8] allow to calculate a complete set of primary yields (Table 3) keeping the writing convention $e^-_{aq} = H_2O^-$ and respecting the fundamental relation

$$3G_{HO_2^\bullet} + 2G_{H_2O_2} + G_{OH^\bullet} = 2G_{H_2} + G_{e^-_{aq}} + G_{H^\bullet} = G_{-\mathrm{water}}. \quad (12)$$

4. Homogeneous secondary reactions

After the primary step, species that have diffused in the whole volume of solution can react with the solvent (H_2O) and its main active solute (OH^-), or between themselves, respectively through at least 7 acido-basic equilibria (Table 4) and about sixty reactions (Table 5). Corresponding to the decomposition of an alkaline water devoid of any other reagent solute, these reactions lead to the secondary production of molecules and radicals, either already known as primary products, either new (O_2, O_3, etc). For a given

Table 3
Set of primary yields for gamma radiation at 25 °C and pH = 13.225 (pore solution) values in molecule/100 eV

G_{H_2}	$G_{e^-_{aq}}$	G_H	G_{OH^-}	G_{-H_2O}[a]	$G_{H_3O^+}$	G_{OH}	$G_{H_2O_2}$	G_{HO_2}
0.4126	2.7813	0.55	0	9.7191	2.7813	2.9651	0.5957	0

[a] $G_{-H_2O} = G_{-water} + 2G_{H_3O^+} - G_{HO_2} \approx G_{-water} + 2G_{e^-_{aq}}$ due to the convention $e^-_{aq} = H_2O^-$.

Table 4
Acido-basic equilibria and rate constants used for radiolytic chemistry within the cement pore solution with ionic strength $I = 0.2257$ mol/kg and water activity = 0.9917

No.	Reactions	Pre-exponential factor A	Activation energy EA (kJ/mol)	$k_{25\,°C}$ ($dm^3\,mol^{-1}\,s^{-1}$)	pK_a 25 °C	Reference
E01	$e^-_{aq} + H_2O = H + OH^- + H_2O$	3.6×10^8	31.7	1.006×10^3	9.77[a]	[12]
E02	$H + OH^- = e^-_{aq}$	1.3×10^{14}	38.4	2.51×10^7		[13]
E03	$O^- + H_2O = OH + OH^-$			1.815×10^6	11.9	
E04	$OH + OH^- = O^- + H_2O$	7.22E9 + 1.62E8T + 2.4E6T^2 − 7.81E3T^3 + 1.06E1T^4[b]		1.265×10^{10}		[14]
E05	$O2[-] + H_2O = HO_2 + OH^-$			1.442×10^{-1}	4.8	
E06	$HO_2 + OH^- = O2[-] + H_2O$	7.22E9 + 1.62E8T + 2.4E6T^2 − 7.81E3T^3 + 1.06E1T^4[b]		1.265×10^{10}		[14]
E07	$H_2O + H_2O = OH^- + H_3O^+$			6.461×10^{-7}	13.9953	
E08	$OH^- + H_3O^+ = 2\ H_2O$	6.62E10 + 1.48E9T + 1.28E7T^2 − 6.03E4T^3 + 1.28E2T^4[b]		1.103×10^{11}		[14]
E09	$O^{2-} + H_2O = 2\ OH^-$			10^{10}	≈36	
E10	$OH^- + OH^- = O^{2-} + H_2O$	Unavailable data		1.005×10^{-10}		Estimation
E11	$HO_2^- + H_2O = H_2O_2 + OH^-$			4.718×10^4	11.684	
E12	$H_2O_2 + OH^- = HO_2^- + H_2O$	1.063×10^{12}	18.8	5.407×10^8		[15]
E13	$O_2^{2-} + H_2O = HO_2^- + OH^-$	3.39×10^8	14.2	1.103×10^6	16.5	[15]
E14	$HO_2^- + OH^- = O_2^{2-} + H_2O$			3.506×10^5		

[a] Theoretic equilibrium, not realized.
[b] Kinetics non defined by Arrhenius law.

species, the kinetic evolution due to secondary reactions results from the observed associations with the other species, as a product or as a reagent. The example of H_2 figures among the simplest

$$\left(\frac{d[H_2]}{dt}\right)_{sec} = +k_1[e^-_{aq}]^2 + k_2[e^-_{aq}][H^\cdot] + k_{12}[H]^2 + k_{13}[H^\cdot][H_2O] \quad \text{(as product)} - k_{22}[O^{\cdot-}][H_2] - k_{31}[OH^\cdot][H_2] \quad \text{(as reagent)}. \tag{13}$$

4.1. Acido-basic equilibria

Owing to the fact that pK_a values of acido-basic couples involved in water radiolysis are clearly lower than the pH of the pore solution (excepted for HO_2^-/O_2^{2-}), all the primary species are mainly converted into their basic equivalent

$$H^\cdot + OH^- \Longleftrightarrow e^-_{aq} \quad pK_a = 9.6\ [9] \tag{14}$$

$$OH^\cdot + OH^- \Longleftrightarrow O^{\cdot-} + H_2O \quad pK_a = 11.9\ [9] \tag{15}$$

$$HO_2^\cdot + OH^- \Longleftrightarrow O_2^{\cdot-} + H_2O \quad pK_a = 4.8\ [10] \tag{16}$$

$$H_2O_2 + OH^- \Longleftrightarrow HO_2^- + H_2O \quad pK_a = 11.68\ [6] \tag{17}$$

$$HO_2^- + OH^- \Longleftrightarrow O_2^{2-} + H_2O \quad pK_a \approx 16.5\ [11]. \tag{18}$$

Reactivity of the new species is distinct, systematically stronger for the e^-_{aq} radical, and generally weaker for the different deprotoned species of oxygen like superoxide radical $O_2^{\cdot-}$, much reactiveless than its homologue $HO_2^\cdot$. As a consequence, $O_2^{\cdot-}$ radical can reach significant concentrations in alkaline solution under irradiation. The case of the radical oxide $O^{\cdot-}$ is similar, except when it attacks H_2 with a kinetic rate three times higher in comparison with the $OH^\cdot + H_2$ reaction. For basic peroxide species, the behaviour is indifferent or not well known (O_2^{2-}). It can be noted that, because of the existence of two equilibria, peroxides speciation at the pH of the pore solution leads to the coexistence of 97.77% HO_2^-, 2.10% H_2O_2 and 0.13 % O_2^{2-}. Through it is marginal, the last species nevertheless has a considerable role in the formation of a solid peroxide (Section 5).

Detailed in Table 4, each equilibrium is presented in the form of a reactions couple for which, at least one of the kinetic constants is known, the other one being inferred from the value of $pK_b (= pK_w - pK_a)$. The couple $H^\cdot/e^-_{aq}$ is a particular case, insofar as the theoretical equilibrium value is not observed because of the simultaneous production of both species at the primary stage. Both 'equilibrium' reactions are described with Arrhenius law when $T < 423$ K [12,13]. For the couples $OH^\cdot/O^{\cdot-}$, $HO_2^\cdot/O_2^{\cdot-}$ and the water equilibrium, Arrhenius law is not really applicable and one of both reactions is described with a polynomial function of the temperature [14].

4.2. Reactions

Reactions collected in Table 5 are usable to describe the radiolysis evolution in a strong alkaline medium. The H_3O^+ ion is logically absent in it, unless otherwise speci-

Table 5
Reactions and rate constants used for radiolytic chemistry within the cement pore solution.; by convention, $e^-_{aq} = H_2O^-$

No.	Reaction	Pre-exponential factor A	Activation energy EA (kJ/mol)	$k_2$5°C[a] ($dm^3\ mol^{-1}\ s^{-1}$)[b]	Reference
R01	$e^-_{aq} + e^-_{aq} H_2 + 2OH^-$	2.33×10^{13}	20.3	6.47×10^9	[14]
R02	$e^-_{aq} + H \rightarrow H_2 + OH^-$	7.2×10^{12}	14.0	2.54×10^{10}	[14]
R03	$e^-_{aq} + O^- \rightarrow 2OH^-$	5.6×10^{11}	7.9	2.31×10^{10}	[14]
R04	$e^-_{aq} + OH \rightarrow H_2O + OH^-$	1.2×10^{13}	14.7	3.19×10^{10}	[14]
R05	$e^-_{aq} + HO_2^- \rightarrow H_2\ O + O^- + OH^-$	1.75×10^{12}	15.4	3.51×10^9	[14]
R06	$e^-_{aq} + H_2O_2 \rightarrow H_2O + OH + OH^-$	7.0×10^{12}	15.6	1.29×10^{10}	[14]
R07	$e^-_{aq} + O_2^- \rightarrow H_2O + O_2^{2-}$	3.1×10^{12}	13.6	1.28×10^{10}	[14]
R08	$e^-_{aq} + HO_2 \rightarrow H_2O + HO_2^-$	3.1×10^{12}	13.6	1.28×10^{10}	[14]
R09	$e^-_{aq} + O_2 \rightarrow H_2O + O_2^-$	5.44×10^{12}	14.17	1.79×10^{10}	[14]
R10	$e^-_{aq} + O_3^- \rightarrow 2OH^- + O_2$			1.6×10^{10}	[16]
R11	$e^-_{aq} + O_3 \rightarrow H_2O + O_3^-$			3.6×10^{10}	[17]
R12	$H + H \rightarrow H_2$	2.36×10^{12}	15.05	5.45×10^9	[14]
R13	$H + H_2O \rightarrow H_2 + OH$			5.5×10^2	[18]
R14	$H + O^- \rightarrow OH^-$			2×10^{10}	[19]
R15	$H + OH \rightarrow H_2O$	3.51×10^{11}	7.77	1.53×10^{10}	[14]
R16	$H + HO_2^- \rightarrow OH + OH^-$	4.2×10^{13}	25.6	1.38×10^9	[20]
R17	$H + H_2O_2 \rightarrow OH + H_2\ O$	1.8×10^{11}	21.1	3.62×10^7	[20]
R18	$H + O_2^- \rightarrow HO_2^-$	7.2×10^{11}	10.6	1.00×10^{10}	[14]
R19	$H + HO_2 \rightarrow H_2O_2$	7.2×10^{11}	10.6	1.00×10^{10}	[14]
R20	$H + O_2 \rightarrow HO_2$	9.57×10^{11}	10.61	1.32×10^{10}	[14]
R21	$H + O_3 \rightarrow OH + O_2$			2.2×10^{10}	[17]
R22	$O^- + H_2 \rightarrow OH^- + H$	3.2×10^{10}	13.8	1.22×10^8	[21]
R23	$O^- + O^- \rightarrow O_2^{2-}$			1.0×10^8	[22]
R24	$O^- + OH \rightarrow HO_2^-$	1.7×10^{11}	7.7	7.61×10^9	[14]
R25	$O^- + HO_2^- \rightarrow OH^- + O_2^-$			4.0×10^8	[9]
R26	$O^- + H_2O_2 \rightarrow O_2^- + H_2O$	3.0×10^{11}	15.6	5.55×10^8	[14]
R27	$O^- + O_2^- \rightarrow O^{2-} + O_2$			6.0×10^8	[23]
R28	$O^- + O_2 \rightarrow O_3^-$	3.5×10^{11}	11.2	3.82×10^9	[24]
R29	$O^- + O_3^- \rightarrow 2\ O_2^-$			7.0×10^8	[23]
R30	$O^- + O_3 \rightarrow O_2^- + O_2$			1×10^9	[25]
R31	$OH + H_2 \rightarrow H_2O + H$	6.31×10^{10}	18.15	4.17×10^7	[14]
R32	$OH + OH \rightarrow H_2O_2$	1.04×10^{11}	7.65	4.75×10^9	[14]
R33	$OH + HO_2^- \rightarrow H_2O + O_2^-$	4.5×10^{12}	15.6	8.32×10^9	[14]
R34	$OH + H_2O_2 \rightarrow H_2O + HO_2$	1.57×10^{10}	15.62	2.88×10^7	[14]
R35	$OH + O_2^- \rightarrow OH^- + O_2$	8.75×10^{11}	10.85	1.10×10^{10}	[14]
R36	$OH + HO_2 \rightarrow H_2O + O_2$	1.04×10^{11}	5.62	1.08×10^{10}	[14]
R37	$OH + O_3^- \rightarrow OH^- + O_3$			2.5×10^9	[26]
R38	$OH + O_3^- \rightarrow HO_2 + O_2^-$			8.5×10^9	[26]
R39	$OH + O_3 \rightarrow HO_2 + O_2$			1.1×10^8	[27]
R40	$O_2^- + HO_2^- \rightarrow O_2 + OH^- + O^-$			8.23×10^{-2}	Estimation
R41	$O_2^- + H_2O_2 \rightarrow O_2 + OH^- + OH$			1.3×10^{-1}	[28]
R42	$O_2^- + O_2^- \rightarrow O2 + O_2^{2-}$	4.89×10^8	52.59	2.99×10^{-1}	[29,14]
R43	$O_2^- + HO_2 \rightarrow O_2 + HO_2^-$	2.44×10^9	8.6	7.60×10^7	[10]
R44	$O_2^- + O_3^- \rightarrow 2O_2 + O^{2-}$			1×10^4	[16]
R45	$O_2^- + O_3 \rightarrow O_2 + O_3^-$			1.5×10^9	[17]
R46	$HO_2 + H_2O_2 \rightarrow O_2 + OH + H_2O$			5×10^{-1}	[28]
R47	$HO_2 + HO_2 \rightarrow O_2 + H_2\ O_2$	1.48×10^9	19.1	6.67×10^5	[14]
R48	$HO_2 + O_3 \rightarrow OH + 2O_2$			5×10^8	[16]
R49	$O_3^- \rightarrow O^- + O_2$	2.75×10^{11}	45.7	2.71×10^3	[14]
R50	$O_3^- + H_3O^+ \rightarrow OH + H_2O + O_2$			9×10^{10}	[26]
R51	$O_3^- + HO_2^- \rightarrow O_2^- + OH^- + O_2$			8.9×10^5	[30]
R52	$O_3^- + H_2O_2 \rightarrow O_2^- + H_2O + O_2$			1.6×10^6	[31]
R53	$O_3 + OH^- \rightarrow O_2 + HO_2^-$			4.8×10^1	[32]
R54	$O_3 + HO_2^- \rightarrow O_2 + OH + O_2^-$			5.5×10^6	[33]
R55	$O_3 + H_2O_2 \rightarrow O_2 + OH + HO_2$	2.8×10^{11}	73.5	3.72×10^{-2}	[34]
R56	$H_2O_2 + HO_2^- \rightarrow H_2O + O_2 + OH^-$			4.5×10^{-4}	[35]

[a] $k = A\ \exp(-EA/RT)$.
[b] Excepted for R49 (s^{-1}).

fied. The list, nonstandard, is principally based on the critical review of Elliot [14], completed by twenty or so contributions [16–35]. Within this comprehensive list, some crossed reactions or feed-back reactions hold the attention in consideration of their regulating role towards radiolysis.

(1) Effective in neutral medium with no poison solute like O_2, the chain reaction leading to the control of the molecular primary products and to the water re-formation is known under the denomination of 'Allen chain' [36]:

$$\text{Initiation}: OH^{\cdot} + H_2 \rightarrow H^{\cdot} + H_2O$$
$$k_{31} = 4.2 \times 10^7\ \text{dm}^3\text{mol}^{-1}\text{s}^{-1} \quad (19)$$
$$\text{Propagation}: H^{\cdot} + H_2O_2 \rightarrow OH^{\cdot} + H_2O$$
$$k_{17} = 3.6 \times 10^7\ \text{dm}^3\text{mol}^{-1}\text{s}^{-1} \quad (20)$$
$$\text{Balance}: H_2 + H_2O_2 \rightarrow 2\ H_2O. \quad (21)$$

Because of the reagents conversion into their basic form, this 'classic' chain is replaced by a strictly equivalent chain in very alkaline medium:

$$\text{Initiation}: O^{\cdot -} + H_2 \rightarrow e^-_{aq}$$
$$k_{22} = 1.2 \times 10^8\ \text{dm}^3\text{mol}^{-1}\text{s}^{-1} \quad (22)$$
$$\text{Propagation}: e^-_{aq} + HO_2^- \rightarrow O^{\cdot -} + OH^- + H_2O$$
$$k_5 = 3.5 \times 10^9\ \text{dm}^3\text{mol}^{-1}\text{s}^{-1} \quad (23)$$
$$\text{Balance}: H_2 + HO_2^- \rightarrow OH^- + H_2O. \quad (24)$$

Characterized by higher kinetic constants (index is related to reaction number in Table 5), this new chain reaction, appears more efficient and faster to reach a steady state where the H_2 concentration becomes stable. Continually, the system then destroys no less H_2 by secondary way that it creates by primary channel. Like in the original chain, the initial condition in solution $[H_2]/[O_2] > 2$ is determining in order to reach the steady state and this latter is easily broken by O_2 poisoning. An alternative chain reaction, even faster than reactions (5) and (22), is then set up:

$$\text{Initiation}: e^-_{aq} + O_2 \rightarrow H_2O + O_2^{\cdot -}$$
$$k_9 = 1.8 \times 10^{10}\ \text{dm}^3\text{mol}^{-1}\text{s}^{-1} \quad (25)$$
$$\text{Propagation}: O^{\cdot -} + O_2^{\cdot -} \rightarrow O^{2-} + O_2$$
$$k_{27} = 6.0 \times 10^8\ \text{dm}^3\text{mol}^{-1}\text{s}^{-1} \quad (26)$$
$$\text{Balance}: e^-_{aq} + O^{\cdot -} \rightarrow H_2O + O^{2-} \rightarrow 2OH^-. \quad (27)$$

Being not regulated, decomposition of the alkaline solution produces H_2 and O_2 (simultaneously) in these conditions.

(2) In alkaline medium, both species of the acido-basic couple H_2O_2/HO_2^- are led to dismute by the reaction (57) [35], with a maximum decomposition rate when $\text{pH} = \text{p}K_a = 11.68$.

$$H_2O_2 + HO_2^- \rightarrow O_2 + OH^- + H_2O$$
$$k_{57} = 4.5 \times 10^{-4}\ \text{dm}^3\text{mol}^{-1}\text{s}^{-1}. \quad (28)$$

In spite of a higher pH of the pore solution and a very low kinetic constant, this reaction is not negligible, especially when the dose rate decreases or when the system is relaxing after the irradiation stops. In this case, reaction (57) can be at the origin of a delayed production of O_2.

(3) More efficient than the previous one, the Haber–Weiss reaction is also a dismutation reaction (between peroxide and superoxide) leading to the O_2 formation. Initially described in acidic medium (reaction 46 [28]), it knows two derived forms in neutral or alkaline medium:

$$H_2O_2 + HO_2^{\cdot} \rightarrow O_2 + OH^{\cdot} + H_2O$$
$$k_{46} = 5 \times 10^{-1}\ \text{dm}^3\text{mol}^{-1}\text{s}^{-1} \quad (29)$$
$$H_2O_2 + O_2^{\cdot -} \rightarrow O_2 + OH^{\cdot} + OH^-$$
$$k_{41} = 1.3 \times 10^{-1}\ \text{dm}^3\text{mol}^{-1}\text{s}^{-1} \quad (30)$$
$$HO_2^- + O_2^{\cdot -} \rightarrow O_2 + O^{\cdot -} + OH^-$$
$$k_{40} = 8.2 \times 10^{-2}\ \text{dm}^3\text{mol}^{-1}\text{s}^{-1}. \quad (31)$$

The kinetic constant of this last reaction, prevailing in the pore solution, is here estimated assuming that the k_{41}/k_{40} ratio is the mean of the constants ratios related to H_2O_2 and HO_2^- observed with the neighbouring radicals $O^{\cdot -}$ and $O_3^{\cdot -}$:

$$\left(\frac{k_{41}}{k_{40}}\right)_{O_2^-} = \sqrt{\left(\frac{k_{26}}{k_{25}}\right)_{O^-}\left(\frac{k_{52}}{k_{51}}\right)_{O_3^-}} \approx 1.59. \quad (32)$$

Not very much sensitive at short term, the effect of reaction 40 limits the accumulation of $O_2^{\cdot -}$ radical when the irradiation duration is long.

5. Calcium peroxide octahydrate precipitation

In the presence of calcium hydroxide, which is widely available within the cementitious matrix, H_2O_2 and its derived species are apt to react for giving a metastable solid phase: the calcium peroxide octahydrate [1]. However, this compound is not formed at the beginning of the irradiation, but only comes when the peroxide accumulation in solution reaches, *a minima*, the solubility product K_{per}. On account of the corrections provided to the speciation of both peroxides and calcium in equilibrium with $Ca(OH)_2$ (respectively, Tables 6 and 2), the K_{per} value is here slightly corrected

$$K_{per} = [Ca^{2+}][O_2^{2-}]^2(H_2O)^8 \cdot \gamma_2^2 = 2.51 \times 10^{-11}. \quad (33)$$

Within the context of an heterogeneous precipitation, directly on the $Ca(OH)_2$ substrate, supersaturation in peroxide ion is not necessary. Considering a concentration $[Ca^{2+}] = 6.9 \times 10^{-4}\ \text{mol dm}^{-3}$ in the pore solution (Table 1), K_{per} is then reached as soon as $[O_2^{2-}] = 4.2 \times 10^{-7}\text{mol dm}^{-3}$, that is for a total concentration $[O_2^{2-}] + [HO_2^-] + [H_2O_2] = 3.35 \times 10^{-4}\ \text{mol dm}^{-3}$. Beyond this threshold, the composition of the pore solution becomes regulated by two minerals:

- $Ca(OH)_2$ (control of total calcium),
- $CaO_2 \cdot 8H_2O$ (control of total peroxide)

Appearance of this mineralogical super-buffer results in a limitation of the chemical variations for the medium under irradiation, especially those related to O_2, and indirectly to H_2, whose net production is regulated through the medium of equilibria and secondary reactions previ-

Table 6
Mineralogical and acido-basic equilibria used in the calculation of the pore solution under irradiation at 25 °C

Species	Equilibrium constant	Value	Ref.
Ca peroxide hexahydrate $CaO_2 \cdot 8H_2O$	$K_{per} = [Ca^{2+}][O_2^{2-}]^2(H_2O)^8 \cdot \gamma_2^2$	$10^{-10.5998}$	This work
Couple H_2O_2/HO_2^-	$K_3 = \frac{[H_2O_2][OH^-]}{[HO_2^-](H_2O)}$	$10^{-2.3112}$	[6]
Couple HO_2^-/O_2^{2-}	$K_4 = \frac{[HO_2^-][OH^-]\gamma_1^2}{[O_2^{2-}](H_2O)\gamma_2}$	$10^{2.5047}$	[11]
Couple $OH^{\cdot}/O^{\cdot -}$	$K_5 = \frac{[OH][OH^-]}{[O^-](H_2O)}$	$10^{-2.0953}$	[9]
Couple $HO_2^{\cdot}/O_2^{\cdot -}$	$K_6 = \frac{[HO_2][OH^-]}{[O_2^-](H_2O)}$	$10^{-9.1953}$	[10]
Couple OH^-/O^{2-}	$K_7 = \frac{[OH^-]^2\gamma_1^2}{[O^{2-}](H_2O)\gamma_2}$	$10^{22.0047}$	Estimated

[a] $(H_2O) = \frac{[H_2O]}{[H_2O]+\sum[\text{solute}_i]}$.

ously evoked. Nevertheless, it no longer can be considered that the cementitious matrix is an anoxic medium under irradiation (special features excepted for initial conditions) as this hypothesis has been previously proposed [1].

Once it is formed, calcium peroxide octahydrate keeps up with the interstitial liquid an equilibrium in the course of which instantaneous variations of matter are limited. Within this scope, the description of the precipitation and the dissolution can make do with the principle of microreversibility stating that the one proceeds contrary to the other at the molecular scale, as summarized in Eq. (34).

$$CaO_2 \cdot 8H_2O_{\downarrow} \underset{k_{prec}}{\overset{k_{diss}}{\rightleftharpoons}} Ca^{2+} + O_2^{2-} + 8H_2O. \tag{34}$$

Dissolution rate being of zero order with regard to the solid phase, and precipitation rate being proportional to the ionic product, this leads to the relation

$$\frac{k_{\text{diss per}k}}{k_{\text{prec per}}} = K_{per}. \tag{35}$$

As a result, instantaneous variation of the solid peroxide and its constituent ions is written

$$\frac{d[CaO_2 \cdot 8H_2O]}{dt} = -k_{\text{diss per}} \cdot S\left(1 - \frac{[Ca^{2+}][O_2^{2-}] \cdot \gamma_2^2 \cdot (H_2O)^8}{K_{per}}\right) \tag{36}$$

$$\frac{\partial[Ca^{2+}]}{\partial t} = \frac{\partial[O_2^{2-}]}{\partial t} = -\frac{d[CaO_2 \cdot 8H_2O]}{dt}. \tag{37}$$

Precipitation and dissolution affecting $Ca(OH)_2$ can be described in the same way. In addition to the term of relative super-saturation (dimensionless, in brackets), the first kinetic equation shows an interfacial solid-solution area S (m^2) and a constant for dissolution kinetics $k_{\text{diss per}}$ (mol dm^{-3} s^{-1} m^{-2}). Because the configuration of the porous network does not allow for the whole solid phase to be instantaneously in equilibrium with the whole interstitial liquid, S value appears relatively independent of the considered volume of material and can be arbitrarily selected. The dissolution constant of $CaO_2 \cdot 8H_2O$, for its part, has not yet been determined; $k_{\text{diss per}}$ could take place between the values characterizing $Ca(OH)_2$ ($k_{\text{diss port}} = 2.2 \times 10^{-4}$ mol dm^{-3} s^{-1} m^{-2} [37]) and a salt a priori rather near and slightly soluble, $CaC_2O_4 \cdot H_2O$ ($k_{\text{diss oxal}} = 3.5 \times 10^{-7}$ mol dm^{-3} s^{-1} m^{-2} [38]).

The synthesis of $CaO_2 \cdot 8H_2O$ which is described in [39] in order to provide a detailed characterization leads to predict a great instability at room temperature (necessity of a preservation at −18 °C). Thereby, decomposition in aqueous medium, out of irradiation, rapidly shows bubbles of nascent O_2 whose origin could be simply the dismutation reaction of H_2O_2 on HO_2^-. From the viewpoint of the pore liquid evolution under irradiation (generation of peroxide species), the balance formation – decomposition comes finally to consider a transitional storage of the oxygen in solid form with a catalytic role for the calcium:

$$Ca(OH)_2 \downarrow + H_2O_2 + 6H_2O \rightarrow CaO_2 \cdot 8H_2O \downarrow \tag{38}$$

$$CaO_2 \cdot 8H_2O \downarrow \rightarrow Ca^{2+} + O_2^{2-} + 8H_2O \tag{39}$$

$$O_2^{2-} + H_2O \rightarrow HO_2^- + OH^- \tag{40}$$

$$H_2O_2 + HO_2^- \rightarrow H_2O + OH^- + O_2 \tag{41}$$

$$Ca^{2+} + 2OH^- \rightarrow Ca(OH)_2 \downarrow \tag{42}$$

$$\text{Balance} : 2H_2O_2 \rightarrow 2H_2O + O_2. \tag{43}$$

6. Gaseous exchanges

After hardening in sealed condition, the cementitious matrix presents a porous network partially occupied by the interstitial liquid. Under these conditions, the complementary porous volume stores residual gases in equilibrium with initial water (N_2 and O_2) and gases formed during the radiolysis (H_2 and O_2). Although it is highly dispersed within the solid phase for forming a network of fractal type, the porous system of the cementitious matrix can be schematized by an equivalent configuration where exchange area is much less developed (Fig. 2) but which allows an easier understanding of the gas transfers. According to the interfacial film theory [40,41] and considering H_2 for example, molecular flux characterizing the interface crossing by gaseous species is given by Eq. (44)

$$J = 10^3 k_{wH_2}([H_2] - [H_2]^*)(\text{mol } m^{-2}\ s^{-1}), \tag{44}$$

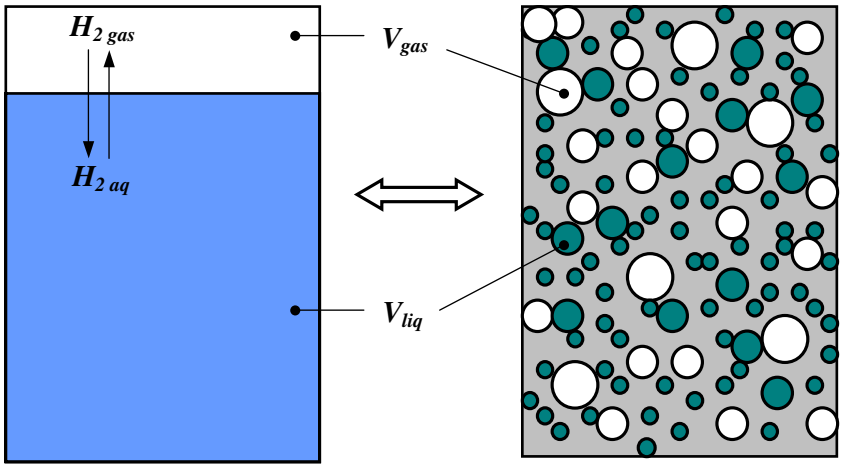

Fig. 2. Schematic representation of the cement paste porosity with its equivalent diphasic configuration (closed system).

where $[H_2]$ is the true concentration in solution (mol/dm^3), $[H_2]^*$ is the virtual concentration in solution at the equilibrium (mol/dm^3) and k_{wH_2} is the interfacial transfer constant for a smooth and at rest interface (m/s).

According to Henry law, concentration in aqueous phase at the equilibrium is given by

$$[H_2]^* = P(H_2) \cdot \frac{[H_2O] + \sum_i [\text{solute}_i]}{K_{H_2}} \ (\text{mol/dm}^3), \tag{45}$$

where K_{H_2} is the Henry law constant (Pa). In addition, for a given gaseous volume, V_{gaz}, it is possible to define a pseudo-concentration of the gaseous species from the amount of matter corresponding to its partial pressure (relation for ideal gases), divided by the solution volume V_{liq}:

$$[H_2g] = P(H_2) \cdot \frac{V_{gas}}{RT} \cdot \frac{1}{10^3 \cdot V_{liq}} \ (\text{mol/dm}^3). \tag{46}$$

Combination of the two previous equations gives a relation between $[H_2]^*$ and $[H_2g]$ allowing to redefine the flux as a function of the amounts of matter present in solution and in gas phase. As transfer kinetics is proportional to flux J and to interfacial area A, kinetics of gaseous exchanges (mol dm^{-3} s^{-1}) is finally described by Eqs. (47) and (48):

$$\left(\frac{d[H_2]}{dt}\right)_{exch} = -\frac{J\mathscr{A}}{10^3 V_{liq}} = -k_{wH_2}\mathscr{A}\left(\frac{[H_2]}{V_{liq}} - \frac{[H_2g]}{V_{gas}} \cdot \frac{10^3 RT([H_2O] + \sum_i [\text{solute}_i])}{K_{H_2}}\right) \tag{47}$$

$$\left(\frac{d[H_2g]}{dt}\right)_{exch} = -\left(\frac{d[H_2]}{dt}\right)_{exch}. \tag{48}$$

Following this model, the description of gaseous exchanges considers that the thickness of liquid covering or filling the pores are low enough to neglect the transport by aqueous diffusion. In return, the ratio between the transfer coefficients of the different gases depends on the value of respective aqueous diffusion coefficients according to the Deacon's theory [40] for a smooth and at rest interface

Table 7
Aqueous diffusion coefficients, interfacial transfer constants and Henry law constants in pure water at 25 °C

Gas	D (m^2/s)	k_w (m/s)	K (Pa)
H_2	4.80×10^{-9} [14]	1.587×10^{-6}	7.1785×10^9 [44]
O_2	2.40×10^{-9} [14]	1×10^{-6} [42]	4.4199×10^9 [45]
N_2	3.05×10^{-9} [43]	1.173×10^{-6}	8.5687×10^9 [46]

$$\frac{k_{w\ \text{gas 1}}}{k_{w\ \text{gas 2}}} = \left(\frac{D_{\text{gas 1}}}{D_{\text{gas 2}}}\right)^{2/3}. \tag{49}$$

Assuming for O_2 gas a transfer constant of the order of 10^{-6} m/s [42], values of k_w for other gases are deduced from Eq. (49). The transfer [14,43] and solubility [44–46] data (Table 7) entitle to infer that H_2, less soluble than O_2, should be also faster than this latter to migrate into the gas phase.

Finally, as the surface of all the meniscus, by definition of the same size because corresponding to a condensation limit (Kelvin–Laplace law), the interfacial area A can be roughly estimated at several thousands of m^2 per kilogram of matrix, after interpretation of the Baroghel-Bouny's work [47] about the material characterization.

7. Simulation of the radiolysis

Integration of previous descriptive elements constitutes the basis of a model from which it is possible to simulate radiolysis with the help of an appropriate calculation tool. With diversified entry formats and a great versatility, *CHEMSIMUL* [48] makes easy the application of this model and allows to carry out different simulations where the previously evoked phenomenologies are coupled (primary production, homogeneous secondary reactions, phase conversion solution/gas or precipitation–dissolution). In order to restrict the number of configurations, it seems judicious to illustrate the behaviour of the Portland cement paste exposed to a gamma irradiation of long duration as a function of three essential parameters: dose rate, pore sat-

uration degree and initial content of H_2 in the porosity. With no connection to a particular application, the pattern studied system is defined by the following characteristics:

- Material: paste of pure Ordinary Portland cement (OPC) with initial mass ratio water/cement $e/c = 0.35$, without entrapped air, cured in sealed system until the hydration degree is maximum (initial cement 83.33 % hydrated); total porosity $n = 0.3188$ occupied at 74.79 % by the interstitial liquid (nominal condition).
- Irradiation: gamma source delivering an homogeneous and constant dose rate in the sealed matrix, without additional space for gas above the material, at 25 °C, during one year; nominal dose rate with respect to water is 0.1 Gy/s.
- Chemistry: composition of the pore solution as defined in Section 6, without extraneous solutes such as carbonate, sulphide, organics, etc; the system is initially in equilibrium with atmosphere, that implies presence of air and water vapour in porosity unoccupied by liquid phase, and a starting concentration $[O_2] = 2.6 \times 10^{-4}$ mol/dm^3 in the pore solution (nominal but penalizing condition); N_2 is considered as inert.

In such a system, the production of radiolytic gases is uniform within the porosity and creates a global variation of pressure without gradient or transport. Evolution of species in the pore solution during the radiolysis of the reference system is represented in Fig. 3. It leads very progressively to an equilibrium state at about one year, after a significant increase of H_2, HO_2^- and $O_2^{\cdot-}$. It is observed that O_2 increases in more moderate proportions, permanently limiting the e_{aq}^- radical at a very low level. Antagonistic of H_2, the $O^{\cdot-}$ radical decreases for its part with the medium enrichment in dihydrogen. In spite of its implication in number of reactions (among them, dismutation), the high level of concentration reached by $O_2^{\cdot-}$ confirms its statute of the less reactive oxygenated radical, all the more in alkaline medium. Within the latter, strongly buffered, none pH variation is observed during radiolysis (H_3O^+ is constant).

In term of gas pressure in the porous volume, doubling of the total pressure with regard to its starting value is due, not only to the formation of H_2, but also to the doubling of the O_2 partial pressure with, at term, $P(O_2) < P(H_2)$ (Fig. 4). Unlike a previous assertion [1], production of O_2 seems then to be possible in a cementitious matrix under irradiation.

7.1. Influence of the pore saturation

For a dose rate equal to 0.1 Gy/s, two new configurations can be derived from the reference's one, characterized by a saturation degree close to 0.75: the first one considers that all the porous volume is occupied by the liquid phase (saturation degree = 1), the second one envisages a partial desiccation so far as to obtain a saturation degree of 0.5. Considering these properties, assumed to be realized at the irradiation beginning, simulations show that in term of total pressure, increase of the gaseous volume is responsible for a delayed equilibrium state, whereas the suppression of this volume is followed, on the contrary, by a swift equilibrium state (Fig. 5). In addition, in the case where sat = 1, the virtual pressure value obtained with the help of Henry law (Section 6) is significantly less than these associated to an unsaturated porosity. In the absence of a buffer reservoir for gases, this result proceeds from the fact that, all of H_2 being available in aqueous phase, attack rate by the $O^{\cdot-}$ radical is maximum (*idem* for O_2 attacked by e_{aq}^-).

An instantaneous rate for H_2 recycling can be defined by Eq. (50)

$$R = 1 - \frac{\left(\frac{d\sum[H_2]}{dt}\right)_{\text{actual}}}{\left(\frac{d[H_2]}{dt}\right)_{\text{primary}}}, \tag{50}$$

where $\sum[H_2]$ refers to the actual concentration of aqueous and gaseous H_2. It can be observed in Fig. 6 that before the equilibrium reaching, R is all the higher since the pore

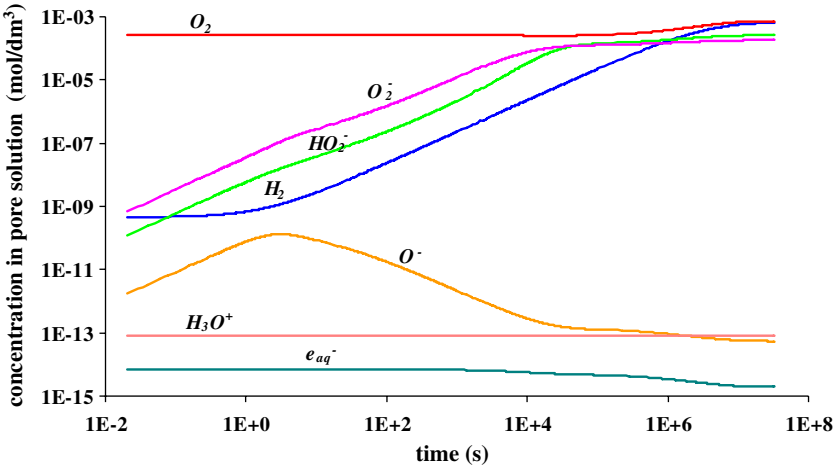

Fig. 3. Evolution of the main radiolytic species as a function of time in a confined cement matrix under gamma radiation at 0.1 Gy/s for a liquid saturation degree of 0.75.

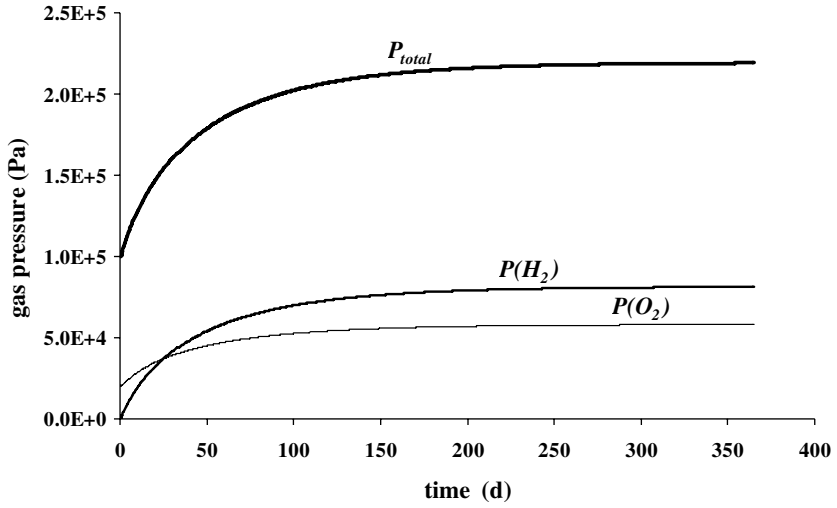

Fig. 4. Evolution of gas pressures as a function of time in a confined cement matrix under gamma radiation at 0.1 Gy/s for a saturation degree of 0.75 (N_2 and H_2O vapour are not plotted).

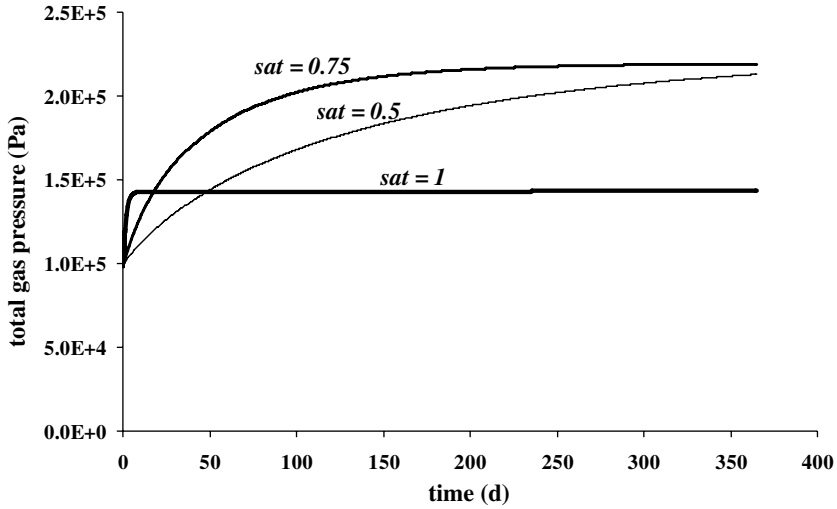

Fig. 5. Comparison of total gas pressures as a function of time for different liquid saturation degrees in a confined cement matrix under gamma radiation at 0.1 Gy/s.

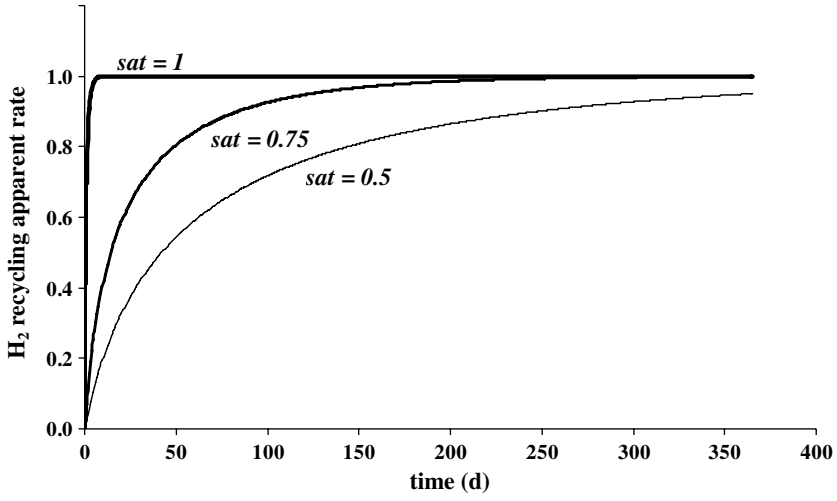

Fig. 6. Comparison of H_2 recycling rates as a function of time for different liquid saturation degrees in a confined cement matrix under gamma radiation at 0.1 Gy/s.

saturation degree is high itself. As a consequence of the mass action law, there is then a possibility to reduce the intensity of the gamma radiolysis and the pressure of gases for the cementitious matrices near the saturation state.

If the possible appearance of $CaO_2 \cdot 8H_2O$ in the system is now considered, the plot of the relative saturation index defined by

$$\sigma = \frac{[Ca^{2+}][O_2^{2-}] \cdot \gamma_2^2 \cdot (H_2O)^8}{K_{per}} - 1 \quad (51)$$

reveals that, at the nominal dose rate of 0.1 Gy/s, precipitation cannot take place, whatever the pore filling by the liquid phase (Fig. 7). The precipitation of calcium peroxide octahydrate does not present then a systematic character and is not, in this case, at the origin of the observed radiolytic equilibrium.

7.2. Influence of the dose rate

For a pore saturation degree set to 0.75, two configurations complete the reference case ($D' = 0.1$ Gy/s), considering successively dose rates of 0.2 and 0.4 Gy/s. Fig. 8 shows that when D' increases, the initial build-up of the total pressure is bigger. On the other hand, conditions leading to an equilibrium state seem to have a different nature when $D' \geqslant 0.2$ Gy/s. In this case, total pressure goes through a maximum and becomes stable after that, all the sooner since D' is higher. Paradoxically, equilibrium pressure seems as the lowest when D' is the highest (0.4 Gy/s). As a consequence, variation of P_{total} is not linear with D' that otherwise suggests the occurrence of a peculiar regulating phenomenon. In term of recycling rate for H_2, Fig. 9 shows also that equilibrium reaching is all the earlier since D' is

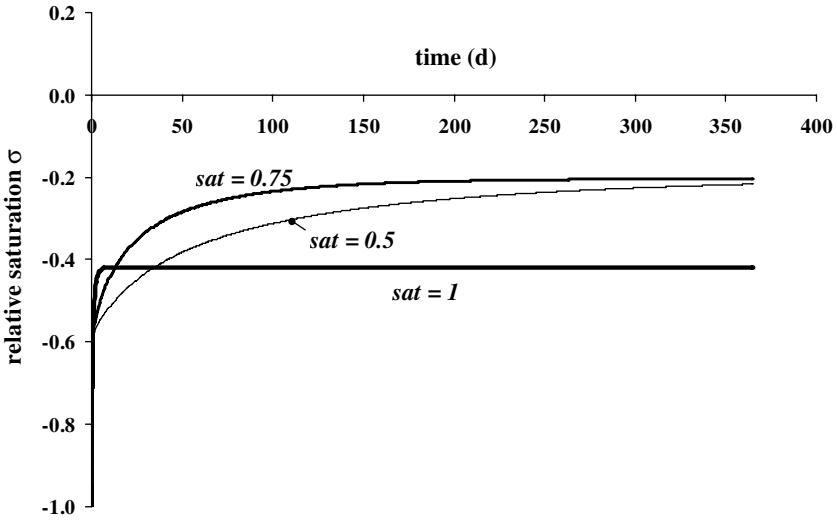

Fig. 7. Evolution of relative saturation index (with respect to $CaO_2 \cdot 8H_2O$ phase) as a function of time in a confined cement matrix under gamma radiation at 0.1 Gy/s for different liquid saturation degrees.

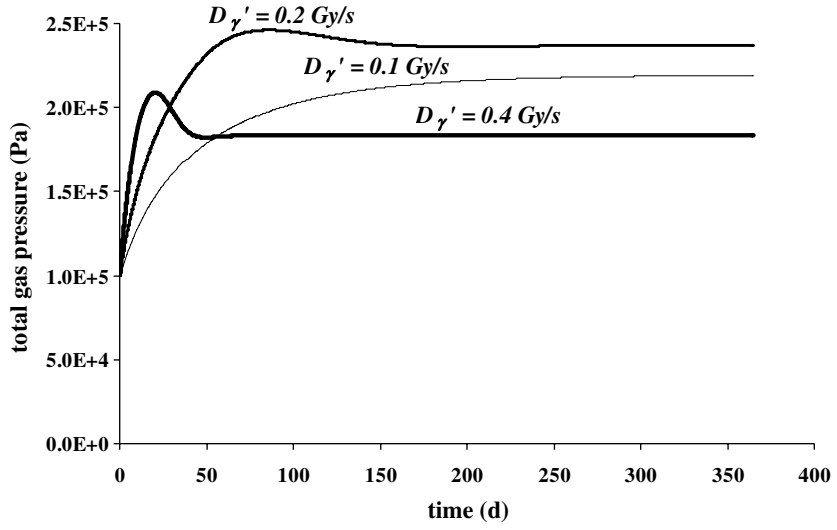

Fig. 8. Comparison of total gas pressures as a function of time in a confined cement matrix under gamma radiation at different dose rates for a liquid saturation degree of 0.75.

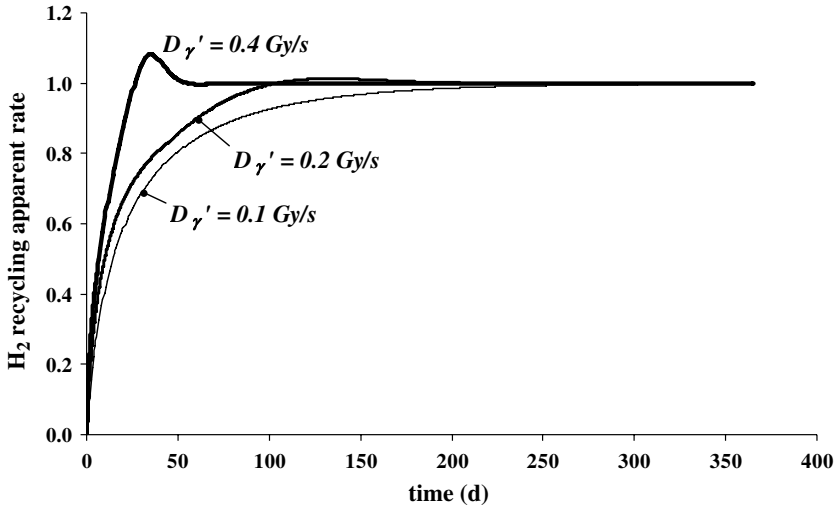

Fig. 9. Comparison of H_2 recycling apparent rates as a function of time at different dose rates in a confined cement matrix under gamma radiation for a liquid saturation degree of 0.75.

higher, with an anomaly for $D' \geqslant 0.2$ Gy/s: stabilization occurs after an episode where the H_2 consumption is greater than the primary production. It can be considered that in the case where $D' = 0.4$ Gy/s, the net resulting destruction of H_2 causes the diminution of the total pressure and its plateau value. Fig. 10 allows to see that this behaviour is related to the $CaO_2 \cdot 8H_2O$ precipitation which occurs after a relatively short time. Although the slight supersaturation momentarily associated to this precipitation quickly impacts P_{total} ($D' = 0.4$ Gy/s), physico-chemical inertia of the system is such that pressure equilibrium arises a lot after the beginning of the precipitation (Fig. 8). At the equilibrium, the amount of precipitated peroxide remains constant, corresponding to few grams, at the maximum, for a volume of pore solution of 1 dm^3 (Fig. 11). Such a small amount decomposes completely in case of irradiation stopping, that has been always seen by X-ray diffraction analysis executed with a time-lag.

Contrary to the interpretation given in [1], the precipitation of $CaO_2 \cdot 8H_2O$ does not make O_2 disappearing, but just leads to a stabilization of this species at a level all the lower since D' is higher. When porosity is totally saturated, simulations carried out at high dose rate (nonrepresented) show in the mean time that the system equilibrium is obtained very quickly without precipitation of calcium peroxide, in fact prevented. Regulating power of the homogeneous reactions system appears then more efficient than the one of the mineralogical control of the solution due to $CaO_2 \cdot 8H_2O$.

7.3. Influence of the initial presence of H_2

Coming back to the reference configuration (sat = 0.75; 0.1 Gy/s) for which the achievement of an equilibrium state is the slowest, a simulation is performed by permuting the starting values of $P(N_2)$ and $P(H_2)$, without modification

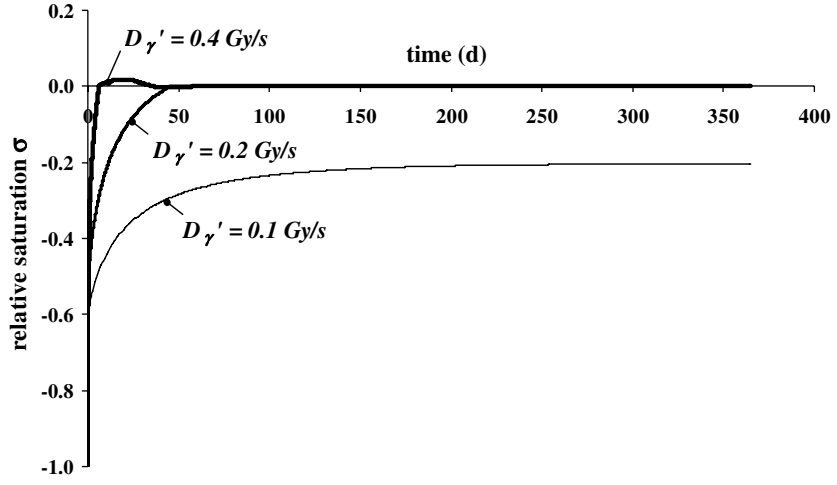

Fig. 10. Evolution of relative saturation index (with respect to $CaO_2 \cdot 8H_2O$ phase) as a function of time in a confined cement matrix under gamma radiation at different dose rates for a liquid saturation degree of 0.75.

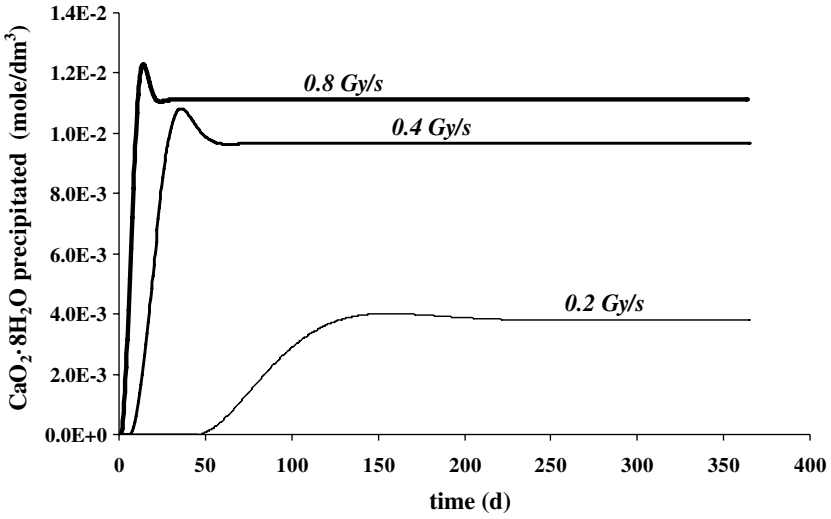

Fig. 11. Amounts of $CaO_2.8H_2O$ precipitated per unit volume of pore solution in a confined cement matrix under gamma radiation at different dose rates for a liquid saturation degree of 0.75.

of $P(O_2)$. After a very fast re-equilibration between gases and pore solution, initial ratio of the concentrations in solution is such as $[H_2]/[O_2] = 3.5$. Evolution of this configuration is particularly spectacular because it leads in less than 1 month to a very different equilibrium from the previous where the $CaO_2 \cdot 8H_2O$ precipitation has no time enough to occur (Fig. 12). After an initial evolution of the species in solution similar to the one seen in Fig. 3, the chemical system shows a general *collapsus* following a large consumption of O_2. After this event, the O_2 concentration is stabilized at a very low value (2.7×10^{-16} mol/dm^3), while the concentrations hierarchy for other species is completely inverted. Fig. 13 shows that in term of pressure, the quasi-disappearance of O_2 is also accompanied by a significant diminution of H_2, the system reaching a depression state. In this configuration, the initial condition $[H_2]/[O_2] > 2$ makes the chain reaction (5)–(22) being highly activated, according to a scenario similar to the one used within the nuclear reactors of the PWR type in order to inhibit radiolysis. It is worthy of note that composition of the system at equilibrium is not very influenced by the dose rate, this one governing only the appearance time (shorter when D' increases).

8. Discussion

Gamma radiolysis of a confined cementitious matrix results from complex mechanisms leading to an equilibrium in a general case. This result is consistent with the oldest experiments [49]. More precisely, the nature of this steady state and the varying characteristics which are related to it show a great sensitivity of the system towards

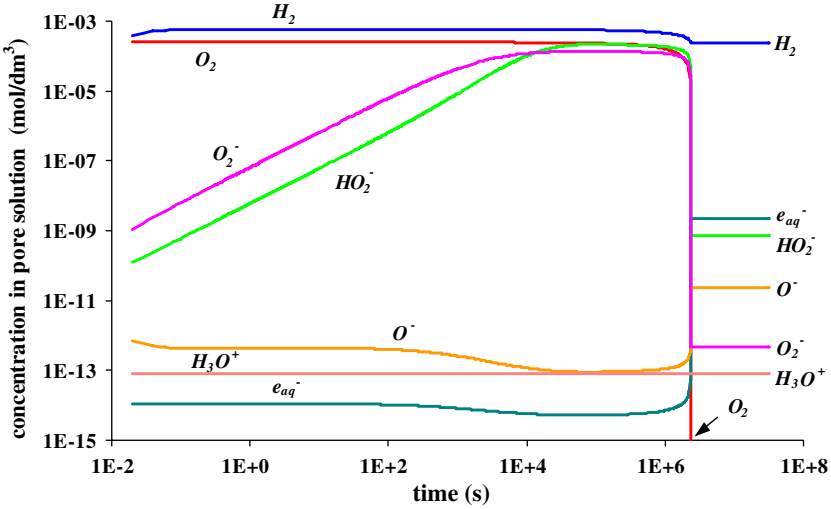

Fig. 12. Evolution of the main radiolytic species as a function of time in a confined cement matrix under gamma radiation at 0.1 Gy/s for a liquid saturation degree of 0.75 with initial H_2.

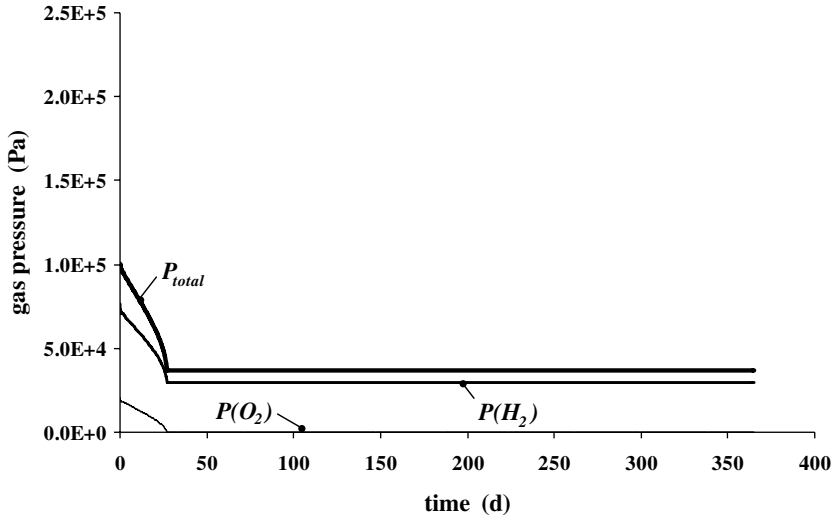

Fig. 13. Evolution of gas pressures as a function of time in a confined cement matrix under gamma radiation at 0.1 Gy/s for a saturation degree of 0.75 with initial H_2 (N_2 and H_2O vapour are not plotted).

initial conditions (dose rate, pore saturation degree or initial composition of the gas phase). When the configuration of the cementitious medium is poorly defined, this unfortunately contributes to diminish the predictive character of the model, both with respect to the time of the equilibrium appearance and with respect to the final state of the system. As a matter of fact, with respect to the initial conditions combination, steady state of the radiolysis proceeds either from a law of mass action on the reactions system in solution, either from the specific activation of the chain reaction (5)–(22), or whether from the mineralogical control of the pore solution by $CaO_2 \cdot 8H_2O$. About this last point, involvement of the calcium peroxide in the O_2 disappearance [1] seems indeed as an erroneous hypothesis because the existence of this phase is obligatory associated to the presence of oxygenated species. As a consequence, it is advisable to provide an another explanation for the O_2 consumption so often observed in cementitious matrices under irradiation [49–51]. From this point of view, oxidation of organic additives or metallic iron issuing from the cement grinding could be a serious cause, especially since it would be able to establish precociously the condition $[H_2]/[O_2] > 2$.

From a classical approach, the model at the basis of this work considers radiolysis of interstitial liquid without the contribution of the porous context, using primary yields and kinetic constants determined in solution. In the light of a recent work about the water radiolysis in porous glasses [52], it seems however that primary mechanisms within an heterogeneous matrix are deeply modified, leading to an exaggerated production of the molecular species H_2 and H_2O_2. Within the pores whose diameter stretches over few nanometers up to several dozens nanometers (that corresponds to intrinsic porosity of the main hydrate phase in OPC pastes), such modifications were previously forecasted [53], noticing the possible interference with the radicals diffusion length, and the effect on their recombination probability. If such a behaviour was demonstrated in cementitious medium, the model could then be dealt with new improvements. For instant, the model remains applicable because it is too early to describe a set of precise mechanisms (do primary yields keep any significance in ultra-confined volumes? is reactivity modified by the surfaces? do chemical events observed in the finest porosity have a consequence on chemical kinetics in the coarse porosity?). It can be also supposed that the existence of the chemical and mineralogical buffers in the cementitious matrix could strongly soften the full significance of phenomena revealed in glasses at neutral pH.

9. Conclusion

Basis mechanisms of the radiolysis in cementitious matrices have been presented in the specific context of gamma irradiation, in closed system, without upper vapour space, and at 25 °C, for a solution representative of an interstitial liquid of Portland cement. All the data collected in support comprise, among other things, a reaction list for radiolysis especially suitable for very alkaline media, as well as a revised description of equilibria related to calcium hydroxide. Under irradiation, the very high pH of the pore solution brings about the generation of basic radiolytic species whose own reactivity remains compatible with the existence of a chain reaction of the Allen type, faster than in neutral medium. Favoured in very alkaline medium, build-up in $O_2^{\cdot-}$ radical moreover encourages to not neglect the Haber–Weiss reactions which are limiting the concentration of this species at long-term. Simulations show that the $CaO_2 \cdot 8H_2O$ precipitation is not systematic, only occurring if preliminary accumulation of peroxide ions is sufficient, which essentially depends on the dose rate. This precipitation becomes critical between 0.1 and 0.2 Gy/s, leading to the appearance of a mineralogical super buffer, constituted by $CaO_2 \cdot 8H_2O$ and $Ca(OH)_2$, which succeeds

in regulating progressively all the species in solution, then in gas phase. Subject to decomposition, solid peroxide does not accumulate, which justifies a description of precipitation–dissolution based on micro-reversibility.

Presence of a gas phase in the material porosity softens the efficiency of the Allen type chain reaction, because it favours the change of H_2 into gaseous form and decreases the H_2/O_2 ratio in solution. On the other hand, complete saturation of the pores results in a H_2 recycling and in an equilibrium state of the system much more efficient that in the presence of solid peroxide, without revealing an anoxic state for all that. Except the initial presence of powerful reducing agents in the cementitious matrix, there is not then an intrinsic evolution under irradiation leading to O_2 disappearance in the presence of calcium (secondary reactions producing O_2 are on the contrary numerous enough). Among the conditions allowing such a disappearance, the initial ratio $[H_2]/[O_2] > 2$ guarantees to arrive at the result, excluding the action of any other regulating mechanism. Appearing time of equilibrium is all the shorter as the dose rate is higher, like in the case of the $CaO_2 \cdot 8H_2O$ precipitation.

In conclusion, cementitious matrix exposed to gamma irradiation in closed system presents different regulating mechanisms able to limit radiolysis effects, or even to make this latter nondangerous (no important pressurization in the material). This behaviour cannot be extrapolated to open systems or alpha irradiation.

References

[1] P. Bouniol, A. Aspart, Cement Concrete Res. 28 (11) (1998) 1669.
[2] P. Bouniol, Etat des connaissances sur la radiolyse de l'eau dans les colis de déchets cimentés et son approche par simulation, Report CEA-R-6069, Direction des systèmes d'information CEA/Saclay, 2004.
[3] IAPS, Release on the ion product of water substance, NBS Washington, may 1980.
[4] IUPAC, Pure Appl. Chem. 74 (11) (2002) 2169.
[5] IUPAC, Solubility Data Series, vol. 52, Pergamon, 1992, p. 114.
[6] E.L. Shock, D.C. Sassani, M. Willis, D.A. Sverjensky, Geochim. Cosmochim. Acta 61 (5) (1997) 907.
[7] E. Hayon, Trans. Faraday Soc. 61 (1965) 734.
[8] M. Haïssinsky, Rendements radiolytiques primaires en solution aqueuse, neutre ou alcaline, Actions chimiques et biologiques des radiations Chap. 11, Masson & Cie, 1967, p. 131.
[9] G.V. Buxton, C.L. Greenstock, W.P. Helman, A. Ross, J. Phys. Chem. Ref. Data 17 (2) (1988) 513.
[10] B.H.J. Bielski, D.E. Cabelli, R.L. Arudi, A. Ross, J. Phys. Chem. Ref. Data 14 (4) (1985) 1041.
[11] J. Jacq, O. Bloch, Electrochim. Acta 15 (1970) 1945.
[12] H.A. Schwarz, J. Phys. Chem. 96 (1992) 8937.
[13] H.P. Han, S.D.M. Bartels, J. Phys. Chem. 96 (1992) 4899.
[14] A.J. Elliot, Rate constants and G-Values for the simulation of the radiolysis of light water over the range 0–300 °C, Report AECL-11073, COG-94-167, AECL Research, 1994.
[15] T. Lundström, H. Christensen, K. Sehested, Radiat. Phys. Chemis. 64 (2002) 29.
[16] B. Pastina, J.A. La Verne, J. Phys. Chem. A 105 (2001) 9316.
[17] K. Sehested, J. Holcman, E.J. Hart, J. Phys. Chem. 87 (1983) 1951.
[18] K.J. Hartig, N. Getoff, J. Photochem. 18 (1982) 29.
[19] E. Bjergbakke, Z.D. Draganic, K. Sehested, I.G. Draganic, Radiochim. Acta 48 (1989) 65.
[20] S.P. Mezyk, D.M. Bartels, J. Chem. Soc. Faraday Trans. 91 (1995) 3127.
[21] B. Hickel, K. Sehested, J. Phys. Chem. 95 (1991) 744.
[22] A.J. Elliot, M.P. Chenier, J. Nucl. Mat. 187 (1992) 230.
[23] K. Sehested, J. Holcman, E. Bjergbakke, E.J. Hart, J. Phys. Chem. 86 (1982) 2066.
[24] A.J. Elliot, D.R. Mc Cracken, Radiat. Phys. Chem. 33 (1989) 69.
[25] E. Bjergbakke, K. Sehested, O.L. Rasmussen, H. Christensen, Input files for computer simulation of water radiolysis, report RIS Ø M-2430, Ris Ø National Laboratory, 1984.
[26] K. Sehested, J. Holcman, E. Bjergbakke, E.J. Hart, J. Phys. Chem. 88 (1984) 269.
[27] K. Sehested, J. Holcman, E. Bjergbakke, E.J. Hart, J. Phys. Chem. 88 (1984) 4144.
[28] J. Weinstein, B.H.J. Bielski, J. Am. Chem. Soc. 101 (1979) 58.
[29] B.H.J. Bielski, Photochem. Photobiol. 28 (1978) 645.
[30] W.D. Felix, B.L. Gall, L.M. Dorfman, J. Phys. Chem. 71 (1967) 384.
[31] G. Czapski, J. Phys. Chem. 71 (1967) 1683.
[32] L. Forni, D. Bahnemann, E.J. Hart, J. Phys. Chem. 86 (1982) 255.
[33] J. Staehelin, J. Hoigne, Environ. Sci. Technol. 16 (1982) 676.
[34] K. Sehested, H. Corfitzen, J. Holcman, E.J. Hart, J. Phys. Chem. 96 (1992) 1005.
[35] F.R. Duke, T.W. Haas, J. Phys. Chem. 65 (1961) 304.
[36] A.O. Allen, C.J. Hochanadel, J.A. Ghormley, T.W. Davis, J. Phys. Chem. 56 (1952) 575.
[37] K. Johannsen, S. Rademacher, Acta Hydrochim. Hydrobiol. 27 (1999) 72.
[38] D.J. White, G.H. Nancollas, J. Crystal Growth 57 (1982) 267.
[39] A. Trokiner, A. Bessière, R. Thouvenot, D. Hau, J. Marko, V. Nardello, C. Pierlot, J.M. Aubry, Solid State Nucl. Magn. Reson. 25 (2004) 209.
[40] E.L. Deacon, Tellus 29 (1977) 363.
[41] P.S. Liss, L. Merlivat, The role of Air–Sea Exchange in Geochemical Cycling, D. Reidel Publishing Company, 1986, p. 113.
[42] M.H. Hutchinson, T.K. Sherwood, Industrial and Engineering Chemistry 29 (1937).
[43] D.L. Wise, G. Houghton, Chem. Eng. Sci. 21 (1966) 999.
[44] C.L. Young IUPAC Solubility Data Series, Vols. 5&6, Pergamon, 1981.
[45] R. Battino IUPAC Solubility Data Series, vol. 7, Pergamon, 1981.
[46] R. Battino IUPAC Solubility Data Series, vol. 10, Pergamon, 1981.
[47] V. Baroghel-Bouny, Caractérisation des pâtes de ciment et des bétons; méthodes, analyse, interprétations, Laboratoire Central des Ponts et Chaussées, Paris 1994.
[48] P. Kirkegaard, E. Bjergbakke, CHEMSIMUL: a simulator for chemical kinetics, Report Risoe-R-1085 (Ed. 2) (EN), Risoe National Laboratory 2005.
[49] N.E. Bibler, E.G. Orebaugh, Radiolytic gas production from tritiated waste forms; gamma and alpha radiolysis studies, Report DP-1459, Savannah River Laboratory 1977.
[50] H.J. Möckel, R.H. Köster, Nucl. Techn. 50 (1982) 494.
[51] K. Brodersen, K. Nilsson, Characterization of radioactive waste forms, volume 1, Report EUR 12077, Commission of the European Communities 1989.
[52] P. Rotureau, J.P. Renault, B. Lebeau, J. Patarin, J.C. Mialocq, Chem. Phys. Chem. 6 (2005) 1316.
[53] P. Offermann, Mater. Res. Soc. Symp. Proc. 127 (1989) 461.